Korean J. Chem. Eng., 33(8), 2478-2485 (2016)
DOI: 10.1007/s11814-016-0094-6

pISSN: 0256-1115
eISSN: 1975-7220

Reaction kinetics for synthesis of isopropyl myristate catalyzed by sulfated titania

Lihua Zhou*, Yu Niu*, Jinbei Yang*,, Chenggang Li*, Xiaoting Guo*, Ling Li*, and Ting Qiu*,†**

*School of Chemical Engineering, Fuzhou University, Fuzhou 350116, Fujian, China
**School of Ocean Science and Biochemistry Engineering, Fuqing Branch of Fujian Normal University, Fuzhou 350300, Fujian, China
(*Received 24 December 2015 • accepted 1 April 2016*)

Abstract−Sulfated titania (SO_4^{2-}/TiO_2) was prepared and characterized by nitrogen adsorption-desorption, FT-IR, thermostability analyzer, XRD and particle size analyzer. The esterification of myristic acid (MA) with isopropanol (IPOH) catalyzed by the solid super acid SO_4^{2-}/TiO_2 was studied. The effect of reaction kinetics conditions such as temperature, stirrer speed, initial mole ratio of alcohol to acid, and catalyst loading on the conversion of myristic acid was investigated. A second-order pseudo-homogeneous model was developed to calculate the rate of the reaction, and then the kinetic parameters were estimated. The calculated values were in agreement with experimental data.

Keywords: Esterification, Isopropyl Myristate, Kinetics, SO_4^{2-}/TiO_2

INTRODUCTION

Isopropyl myristate (IPM) is a dry and soft non-oily emollient that is used as an excellent solvent for mineral oil, silicone, and lanolin [1,2]. With its good characteristics in absorption, isopropyl myristate is also widely used in cosmetics as the oil component for which excellent distribution properties and good absorption through the skin are required [3]. Because of these excellent characteristics, the preparation of IPM has obtained sustainable research focus.

Conventionally, IPM is synthesized by esterification of myristic acid with isopropanol in the presence of p-toluene sulphonic acid (*p*-TSA) or sulfuric acid [4,5]. Despite strong catalytic activity, the *p*-TSA and sulfuric acid suffers several drawbacks, such as the existence of side reactions, equipment corrosion and environmental pollution. The solid acid catalysts are proposed to solve the problem of homogeneous catalysts. The main advantages of heterogeneous catalysts are low equipment corrosion, no environmental pollution, high selectivity, and ease of separation [6]. Therefore, heterogeneous catalysts such as ion exchange resins have been widely used in esterification and transesterification reactions [7-9]. But the ion exchange resin catalysts also have some drawbacks, such as low thermal stability, low surface area, and solubility in polar media [10]. Especially, they cannot be used in a high reaction temperature due to their low thermal stabilities.

Sulfated titania (SO_4^{2-}/TiO_2) is classified as a heterogeneous catalyst that has both active Brønsted and Lewis acidic sites [11]. Compared with ion exchange resins and other heterogeneous acid catalysts, SO_4^{2-}/TiO_2 shows higher catalytic activity and better thermal stability [12]. The esterification of fatty acids with methanol and transesterification of vegetable oils with methanol using SO_4^{2-}/TiO_2 as catalyst has been studied [13-18], and it is found that SO_4^{2-}/TiO_2 behaves good catalytic activity and stability in the reactions.

The kinetics of esterification of myristic acid with the isopropanol by homogeneous and heterogeneous catalysts was investigated by Yalcinyuca [5], and the results revealed that Amberlyst 15 and silica-based Deguessa could nearly not increase the reaction rate and the conversion of reactants. However, to the best of our knowledge, there have not been kinetic mechanisms related to the esterification of myristic acid using heterogeneous catalysts in the literature. In this paper, the kinetic behavior of the esterification of myristic acid with isopropanol was studied with SO_4^{2-}/TiO_2 as catalyst, the corresponding kinetic parameters were obtained, and their kinetic mechanisms were discussed.

EXPERIMENTAL SECTION

1. Materials.

Isopropyl myristate (mass purity≥98%) and TiO_2 (mass purity≥99%) were supplied by Aladdin, China. Myristic acid (mass purity≥98%) and isopropanol (mass purity≥99.7%) were purchased from Sinopharm Group Co. Ltd. China, and used without further purification. The purities of materials were checked by gas chromatography (GC). N, N-Dimethylformamide was used as internal standard for GC analysis. Deionized water was prepared in our laboratory.

2. Preparation and Characterization of Sulfated Titania (SO_4^{2-}/TiO_2)

2-1. Preparation of Sulfated Titania (SO_4^{2-}/TiO_2)

Sulfated titania was prepared by impregnation method. The 1 $mol \cdot L^{-1}$ sulfuric acid solution was prepared by sulfuric acid and water. TiO_2 and sulfuric acid solution were mixed with a mass ratio of 1 : 2 and then ground for 30 min at room temperature. After filtering, the SO_4^{2-}/TiO_2 was dried in vacuum oven at 363.15 K for 3 h, and then calcined at 625.15 K for 3 h.

2-2. Characterization of Sulfated Titania (SO_4^{2-}/TiO_2)

Nitrogen adsorption-desorption isotherms were measured on ASAP2020 specific surface area analyzer. BET surface areas and pore

†To whom correspondence should be addressed.
E-mail: tingqiu@fzu.edu.cn

size distributions were calculated from the adsorption isotherms using BET model. FT-IR pyridine adsorption measurements were recorded using a Spectrum 2000 FT-IR absorption spectrometer (PerkinElmer Inc., American) for KBr pellets in the frequency range form of 4,000-400 cm^{-1}. The STA449C thermostability analyzer was employed to determine the thermostability of sulfated titania. The crystal forms of sulfated titania were obtained on Rigaku D/max-1200 X-Ray powder diffractometer (XRD). The mean diameter of the catalyst powder was determined by LS230 particle size analyzer.

3. Experimental Apparatus and Procedure for Isopropyl Myristate Synthesis

Isothermal batch kinetic experiments were conducted in a stainless steel reactor of 500 ml equipped with agitation and temperature control device (±0.1 K) (see Fig. 1). An HPLC pump was used for injection of the isopropanol into the reactor.

The desired amount mixture of myristic acid and catalyst was first charged into the reactor. After the reactor was sealed, the reactant and catalyst were heated to the desired temperature with a stirring speed of 100 rpm. Nitrogen was introduced into the reactor to ensure the reactants remained liquid under the desired reaction temperature. Thereafter, the preheated isopropanol was fed into the reactor quickly through the HPLC pump. The time at which the isopropanol was added was considered as the initial time for the reaction. Samples of 2 ml were withdrawn through a sampling line at a different time during a run. To prevent further reaction, the samples were cooled rapidly at 293.15 K. Then, the samples were centrifuged to separate the solid catalyst from the liquid. By analyzing the concentration of the obtained samples, we determined chemical equilibrium in the reaction.

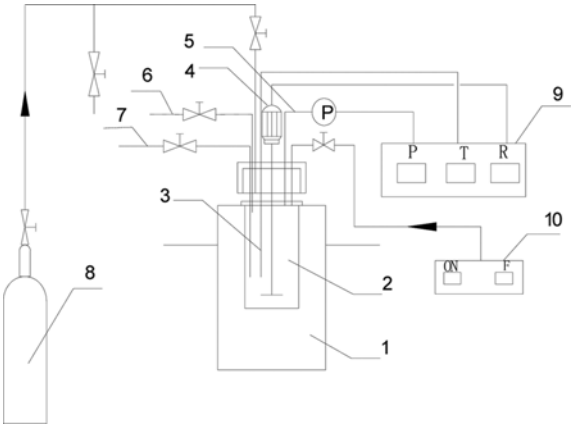

Fig. 1. Apparatus of kinetic experiment.

1. Heating mantle
2. Stainless steel reactor
3. Thermocouple
4. Mechanical stirrer
5. Pressure tap
6. Exhaust valve
7. Sampling valve
8. Nitrogen cylinder
9. Control cabinet
10. HPLC pump

4. Analysis

The isopropyl myristate and isopropanol were analyzed by gas chromatograph (GC-2014) equipped with hydrogen flame ionization detector (FID) and a fused silica capillary column (30 m×0.25 mm×0.25 μm). The FID temperature and the injector temperature were 543.15 K and 533.15 K, respectively. The column temperature was first kept at 313.15 K for 1 min, then increased at 10 K·min^{-1} to 353.15 K, and finally increased at 40 K·min^{-1} to 493.15 K and kept for 1 min. Nitrogen was used as carrier gas at 1.0 ml·min^{-1}. The N, N-Dimethylformamide was used as internal standard. The water concentration was determined by Karl-Fischer titration using WS-3 Coulometer (Xian YunYi instrument Co., LTD, China). In addition, the myristic acid concentration was checked by titration with 0.1 N sodium hydroxide (NaOH) using phenolphthalein as indicator. The acidity (AD) of the sample was calculated as follows:

$$AD = \frac{C_{NaOH} \times V_{NaOH} \times M_A}{m \times 1000} \times 100(wt\%) \quad (1)$$

where C_{NaOH} is the concentration of NaOH, mol·L^{-1}; V_{NaOH} is the volume of NaOH consumed, ml; m is the weight of sample, g; M_A is the molecular weight of myristic acid. The conversion of myristic acid, X_A, can be calculated by Eq. (2):

$$X_A = \left(1 - \frac{AD}{AD_0}\right) \times 100 \quad (2)$$

where AD and AD_0 are the acidity and the initial acidity of the reacting mixture, respectively.

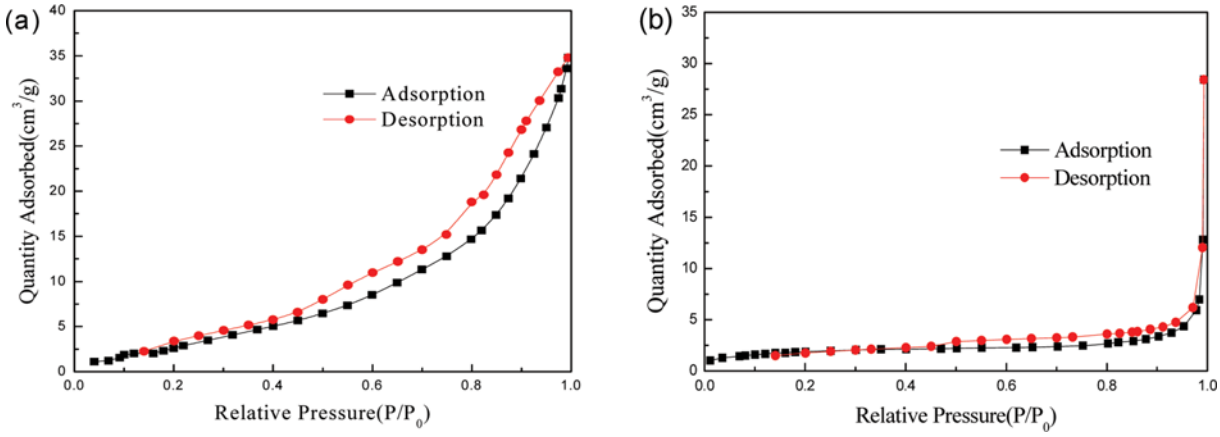

Fig. 2. N_2 adsorption-desorption isotherms of (a) TiO_2 and (b) SO_4^{2-}/TiO_2.

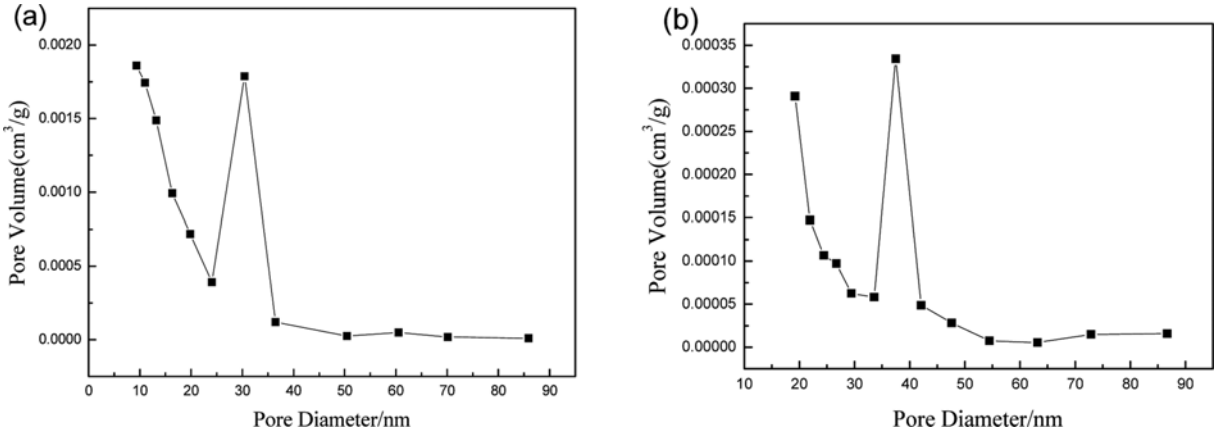

Fig. 3. Pore diameter distribution of (a) TiO_2 and (b) SO_4^{2-}/TiO_2.

RESULTS AND DISCUSSION

1. Characterization of Sulfated Titania

1-1. Nitrogen Adsorption-desorption

Pure titanium dioxide powder (TiO_2) was used as empty medium. Fig. 2 shows the N_2 adsorption-desorption isotherms of TiO_2 and SO_4^{2-}/TiO_2. The surface areas and pore diameter distributions are depicted in Fig. 2.

From Fig. 2(a) and 2(b), the isotherms of TiO_2 and SO_4^{2-}/TiO_2 are the typical mesoporous solid adsorption isotherms with the IV type feature. And the two samples both show an apparent H4 hysteresis loop, signifying that TiO_2 and SO_4^{2-}/TiO_2 have mesoporous structures. As depicted in Fig. 3(b), the pore size of SO_4^{2-}/TiO_2 is concentrated in the range of 35-40 nm, confirming that the prepared catalyst is mesoporous material.

The surface area and pore size are summarized in Table 1. As can be seen, the average pore size increased from 40.55 nm to 53.13 nm after impregnating, which may be caused by the losing of S during high temperature calcination. Correspondingly, the surface area decreased to 46.91 $m^2 \cdot g^{-1}$ from 81.60 $m^2 \cdot g^{-1}$. Besides, the agglomeration of catalyst particles during roast also led to the decrease of surface area.

Table 1. BET analysis results of SO_4^{2-}/TiO_2

Samples	Surface area ($m^2 \cdot g^{-1}$)	Pore size (nm)
Empty medium (TiO_2)	81.60	40.55
SO_4^{2-}/TiO_2	46.91	53.13

1-2. FT-IR Pyridine Analysis

The FT-IR spectrum of SO_4^{2-}/TiO_2 is shown in Fig. 4(a). The peak at 1,635 cm^{-1} is assigned to the deformation vibration of H-O-H of adsorbed water, indicting that the catalyst is bibulous. There was no S=O stretching vibration of SO_4^{2-} in the range of 1,620-1,630 cm^{-1}, signifying no metal in the form of sulfate. All peaks in the region of 1,040-1,080, 1,130-1,150 and 1,200-1,280 cm^{-1} can be attributed to characteristic absorption peaks of SO_4^{2-}/M_XO_Y. Particularly, the peak at 1,227 cm^{-1} represents the super acidity of the prepared catalyst.

The pyridine adsorbed IR spectrum of catalyst is displayed in Fig. 4(b). The prepared catalyst contains Lewis (L) acid (1,448 cm^{-1}) and Brönsted (B) acid (1,547 cm^{-1}). The peak at 1,482 cm^{-1} belongs to the summation characteristic absorption peak of L & B acid. The synergism of Lewis acid and Brönsted acid formed a super acid

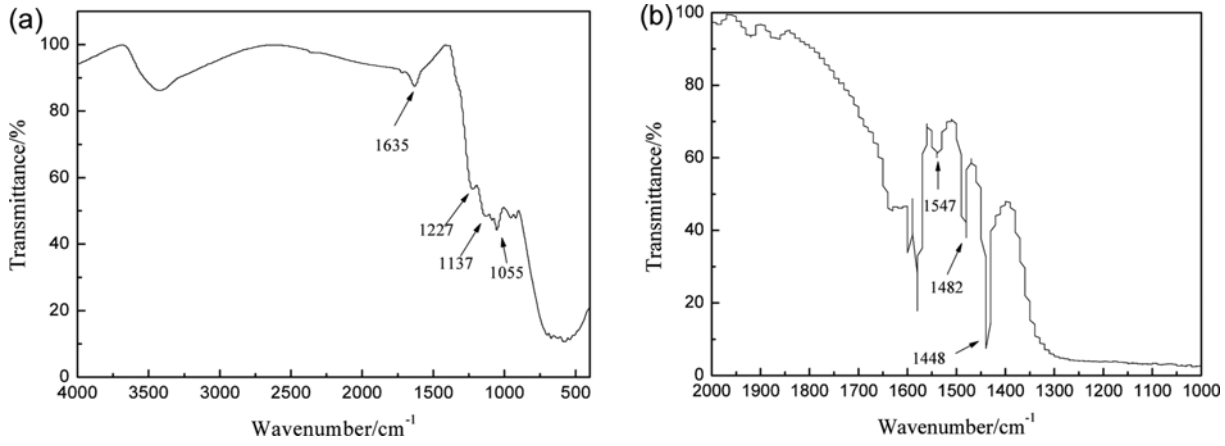

Fig. 4. FT-IR spectrum of (a) SO_4^{2-}/TiO_2 and (b) SO_4^{2-}/TiO_2 with Pyridine adsorbed.

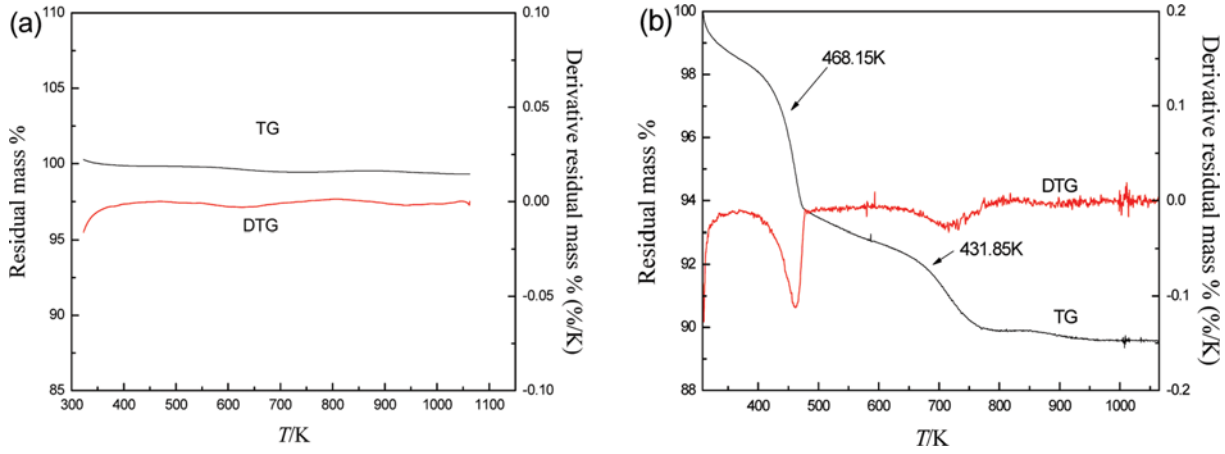

Fig. 5. Thermostability of (a) TiO_2 and (b) SO_4^{2-}/TiO_2.

center, denoting that the prepared catalyst possesses super acidity.

1-3. Thermostability Analysis

Thermostability is one of the important catalyst properties. Fig. 5 shows the thermostability analysis results of TiO_2 and SO_4^{2-}/TiO_2. From Fig. 5(a), there was almost no mass loss for pure TiO_2 at the measurement temperature range (300-1,100 K). As for Fig. 5(b), the mass of sample decreased gradually at relative low temperature due to the loss of physical absorbed water on the surface of catalyst. The mass of sample decreased obviously and a sharp peak appeared on DTG curve at 468.15 K, owing to the loss of some free-S and bonded-S. At 705.15 K, the decomposition of SO_4^{2-} occurred, and the total mass loss was about 10%. However, the mass of sample decreased very slightly when the temperature was higher than 800 K. Thus, it can be said that there was no decomposition of the prepared catalyst when the temperature was lower than 468.15 K.

1-4. XRD Analysis

The XRD patterns of pure TiO_2 and SO_4^{2}/TiO_2 are shown in Fig. 6. Both samples show almost the same peak positions. The pure TiO_2 resulted in four intense diffraction peaks at 25.275°, 38.601°, 55.106° and 62.165°. Compared with the standard XRD spectra, the TiO_2 is anatase phase. After being impregnated and calcined at 350 °C, the TiO_2 displayed three guard diffraction peaks in the 37-40° region. And the three diffraction peaks are the standard XRD peaks of anatase crystal. Additionally, a more sharp diffraction peak appeared at 48.074°, which suggested that there was no conversion of crystal type. Moreover, the anatase phase tends to be more perfect, and the high catalytic activity was consistent with the experimental results.

Besides, the mean diameter of the catalyst powder was 9.95 μm, which was determined by LS230 particle size analyzer. The particle size distribution of SO_4^{2-}/TiO_2 was shown in Fig. 7.

2. Reaction Kinetics

2-1. Elimination of Mass Transfer Resistances

The effect of external diffusion limitation on the esterification reaction is directly related to the stirring speed. As shown in Fig. 8, the conversion rate is independent of the stirring speed which indicates that the external diffusion is not the rate controlling step. The conversion of myristic acid increased with increase in stirring speed from 100 to 300 rpm while keeping all other parameters constant. However, there is no significant effect of stirring speed after 300 rpm. Therefore, all the further kinetic experiments were performed at the constant stirring speed of 300 rpm to eliminate the external mass transfer resistances. Since the solid super acid $SO_4^{2-}/$

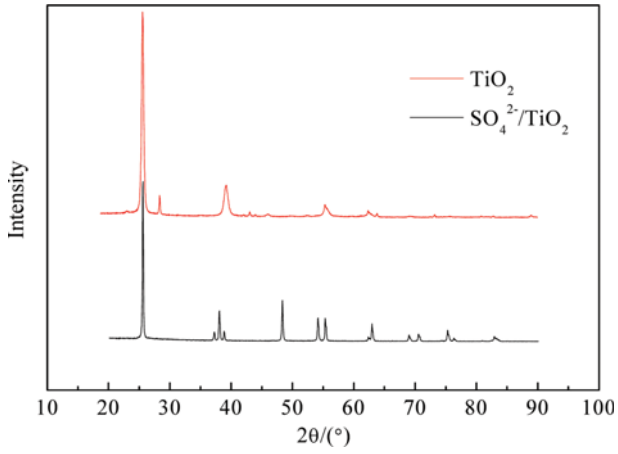

Fig. 6. XRD patterns of TiO_2 and SO_4^{2}/TiO_2.

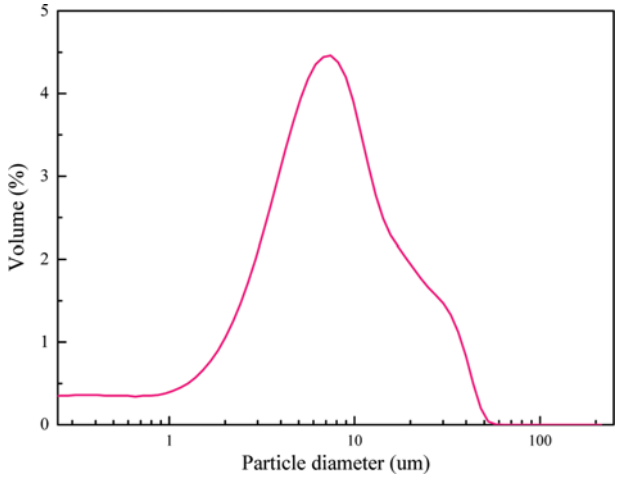

Fig. 7. The particle size distribution of SO_4^{2-}/TiO_2.

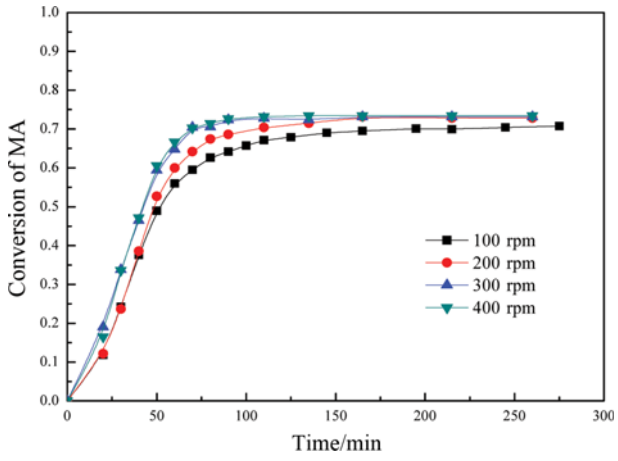

Fig. 8. Effect of stirring speed on the conversion of myristic acid, X_A. Conditions: catalyst, SO_4^{2-}/TiO_2; reaction temperature, 403.15 K; catalyst loading, 5 wt%; initial mole ratio of isopropanol to myristic acid, 2 : 1.

TiO_2 is a powder catalyst, the internal diffusion resistance could be ignored.

2-2. Effect of Reaction Temperature

The reaction temperature, a very important factor for kinetic study, is useful in calculating the activation energy for the reaction. The reaction was performed under various reaction temperatures, from 383.15 to 413.15 K while keeping other parameters constant. The effect of temperature is presented in Fig. 9. The conversion and reaction rate of myristic acid were found to increase with the increment of the reaction temperature. The increasing temperature is obviously favorable for the acceleration of the forward reaction. But the equilibrium conversions under different reaction temperatures change slightly. This indicates that the synthesis of isopropyl myristate from myristic acid and isopropanol is a weakly endothermic reaction.

The equilibrium constant can be calculated from the equilibrium

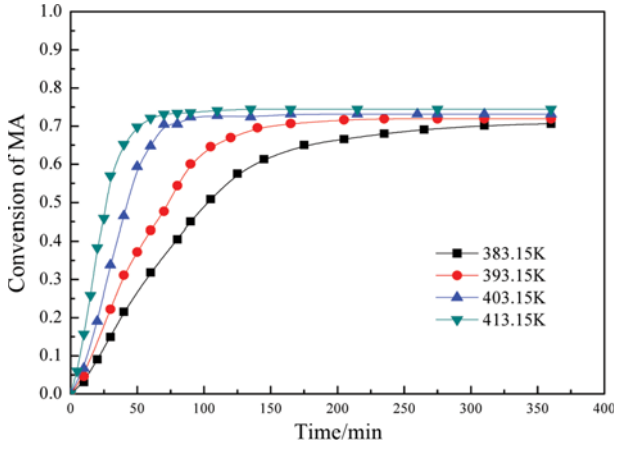

Fig. 9. Effect of reaction temperature on the conversion of myristic acid, X_A. Conditions: catalyst, solid super acid SO_4^{2-}/TiO_2; stirring speed, 300 rpm; catalyst loading, 5 wt%; initial mole ratio of IPOH to MA, 2 : 1.

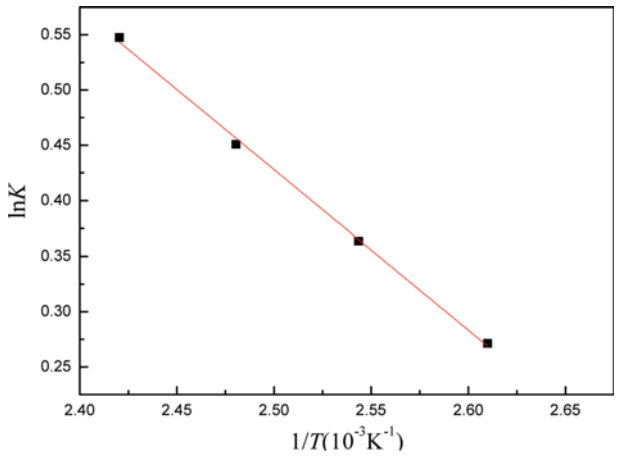

Fig. 10. Temperature dependencies of the equilibrium constant.

concentration:

$$K_{eq}=\frac{k_+}{k_-}=\frac{C_R C_S}{C_A C_B}=\frac{X_A^2}{(1-X_A)(R_n-X_A)} \quad (3)$$

where k_+ and k_- are the forward rate constant and the backward rate constant, respectively. C_A, C_B, C_R, and C_S are the equilibrium concentrations of myristic acid, isopropanol, isopropyl myristate and water, respectively.

The van't Hoff equation gives:

$$\frac{d\ln K}{dT}=\frac{\Delta H}{RT^2} \quad (4)$$

or

$$\ln K=\frac{-\Delta H}{RT}+C \quad (5)$$

where ΔH is the heat of reaction, $J\cdot mol^{-1}$.

The plot of lnK versus 1/T is shown in Fig. 10. The temperature dependence of the equilibrium constant can be given by Eq. (6):

$$K=0.5737\times 10^2 \exp\left(-\frac{-12044.4}{RT}\right) \quad (6)$$

A satisfactory linear coefficient of 0.9981 was obtained. The heat of reaction is estimated, 12.04 $kJ\cdot mol^{-1}$, which indicates that the reaction is a weak endothermic reaction.

2-3. Effect of Catalyst Loading

The amount of catalysts was varied from 1 to 7 wt% to evaluate its effect on the conversion of MA. The higher the catalyst loading, the faster the reaction rate obtained, because it offers more active catalytic sites for the reaction. As can be seen from Fig. 11, the reaction rate of MA increased with an increase in catalyst loading from 1 to 5 wt%. Furthermore, using 7 wt% catalyst did not improve the reaction rate any more. Therefore, further kinetic experiments were performed at catalyst loading of 5 wt%.

2-4. Effect of Reactant Molar Ratio

The esterification reaction is an equilibrium-limited chemical reaction. The use of an excess of reactants may be favorable for forward reaction. The initial molar ratio of IPOH to MA ranging from 1 : 1 to 4 : 1 was investigated and displayed in Fig. 12. It was observed

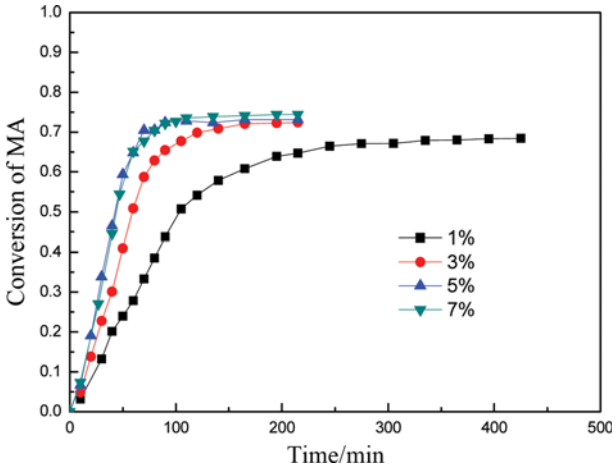

Fig. 11. Effect of catalyst loading on the conversion of MA, X_A. Conditions: catalyst, SO_4^{2-}/TiO_2; stirring speed, 300 rpm; reaction temperature, 403.15 K; initial mole ratio of isopropanol to myristic acid, 2 : 1.

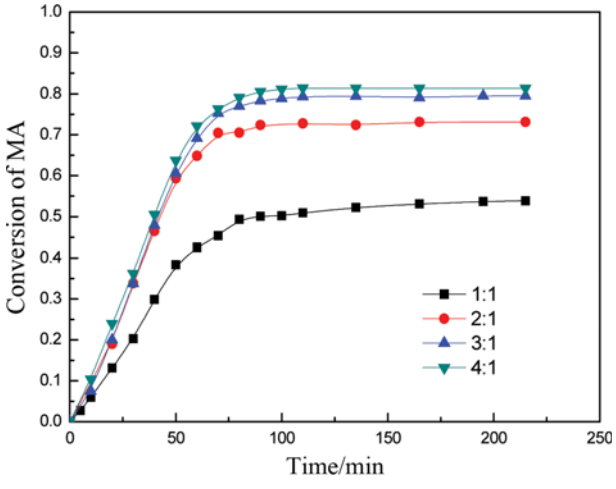

Fig. 12. Effect of reactant molar ratio on the conversion of MA, X_A. Conditions: catalyst, SO_4^{2-}/TiO_2; stirring speed, 300 rpm; reaction temperature, 403.15 K; catalyst loading, 5 wt%.

that the MA conversion and reaction rate were both increased with the increase of the initial reactant molar ratio. It should also be noted that the rise in the initial molar ratio of IPOH to MA from 1 : 1 to 3 : 1 resulted in significant increase of the final conversion.

2-5. Reaction Mechanism

The esterification reaction mechanism of fatty acid with alcohol is similar to that of proton acid. So, the possible esterification reaction mechanism of myristic acid with isopropanol catalyzed by SO_4^{2-}/TiO_2 was determined as follows:

Step 1

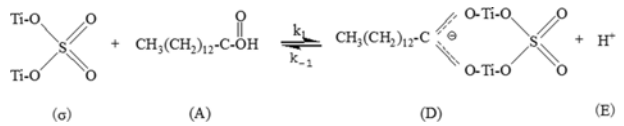

Step 2

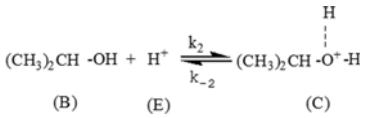

Step 3

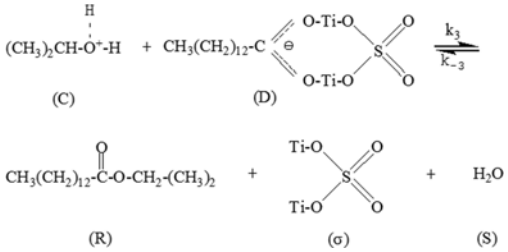

Step 1 and step 2 are relatively fast reactions, and are always assumed to be in chemical equilibrium. But Step 3 is the slowest process and considered as a rate-controlling step.

2-6. Kinetic Modeling

Based on the mechanism of the reaction as mentioned above, a kinetic model can be determined:

$$r = r_3 = \frac{dC_A}{dt} = k_3 C_C \theta_D - k_{-3} C_R C_S (1-\theta_D) \tag{7}$$

where k_3 and k_{-3} are the forward and reverse reaction rate constants of step 3, respectively. And the fractional coverage θ_D is defined as the fraction of total surface adsorption sites that are occupied by D.

As adsorption and nucleophilic substitution reaction are relatively fast, and considered to be in equilibrium, the rates of the reactions can be expressed as:

$$r_1 = k_1 C_A (1-\theta_D) - k_{-1} C_E \theta_D = 0 \tag{8}$$

$$r_2 = k_2 C_E C_B - k_{-2} C_C = 0 \tag{9}$$

where k_1, k_{-1} are the forward and reverse reaction rate constants of Step 1, respectively; k_2 and k_{-2} are the forward and reverse reaction rate constants of Step 2, respectively.

Substitution of Eq. (8) and (9) into Eq. (7) gives:

$$\frac{dC_A}{dt} = k_+'(1-\theta_D)\left[C_A C_B - \frac{C_R C_S}{K_{eq}}\right] \tag{10}$$

where $k_+' = \frac{k_1 k_2 k_3}{k_{-1} k_{-2}}$ and $K_{eq} = \frac{k_1 k_2 k_3}{k_{-1} k_{-2} k_{-3}}$.

Since $C_A = C_{A0}(1-X_A)$, $C_B = C_{A0}(R_n - X_A)$, and $C_R = C_S = C_{A0} X_A$, Eq. (10) can be written as:

$$\frac{dX_A}{dt} = k_+' C_{A0}(1-\theta_D)\left[(1-X_A)(R_n - X_A) - \frac{X_A^2}{K_{eq}}\right] \tag{11}$$

where C_{A0} is the initial concentration of myristic acid, C_{B0} is initial concentration of isopropanol, R_n is the initial molar ratio of isopropanol to myristic acid.

Since the solid super acid SO_4^{2-}/TiO_2 has large specific surface area, the adsorption of myristic acid on catalyst surface is regarded as a strong and fast reaction. Supposing θ_D maintained at a high level, the value of $(1-\theta_D)$ can be considered as a constant. There-

Table 2. Reaction rate constant k_+ and k_- at different temperatures

T/K	10^3k_+	$\ln k_+$	10^3k_-	$\ln k_-$
383.15	1.90	−6.27	1.45	−6.54
393.15	3.00	−5.81	2.08	−6.17
403.15	5.60	−5.18	3.57	−5.64
413.15	9.10	−4.70	5.26	−5.24

fore, Eq. (11) can be written as:

$$\frac{dX_A}{dt} = k_+ C_{A0}\left[(1-X_A)(R_n - X_A) - \frac{X_A^2}{K_{eq}}\right] \quad (12)$$

where $k_+ = k_+'(1-\theta_D)$.

2-7. Estimation of the Reaction Rate Constants

The relationship between rate constant k and temperature T can be expressed by the Arrhenius equation:

$$k = A\exp\left(-\frac{Ea}{RT}\right) \quad (13)$$

or

$$\ln k = -\frac{E_a}{RT} + \ln A \quad (14)$$

where E_a is the activation energy, $J\cdot mol^{-1}$, and A is the pre-exponential factor or apparent frequency factor, $L\cdot min^{-1}\cdot mol^{-1}$.

Since Eq. (12) is nonlinear, a fourth-order Runge-Kutta method is used to calculate the conversion of myristic acid under different time. An objective function is to minimize the squared differences between the calculated values X^{cal} and the experimental values X^{exp}, as shown in Eq. (15). The optimal parameters for the kinetics are estimated by using the Nelder-Mead simplex method, as shown in Table 2.

$$OF = \sum_{i=1}^{n}(X^{exp} - X^{cal})^2 \quad (15)$$

According to Eq. (14), the relationship between ln k and 1/T is presented in Figs. 13 and 14, and E_a and A of k_+ and k_- can be obtained.

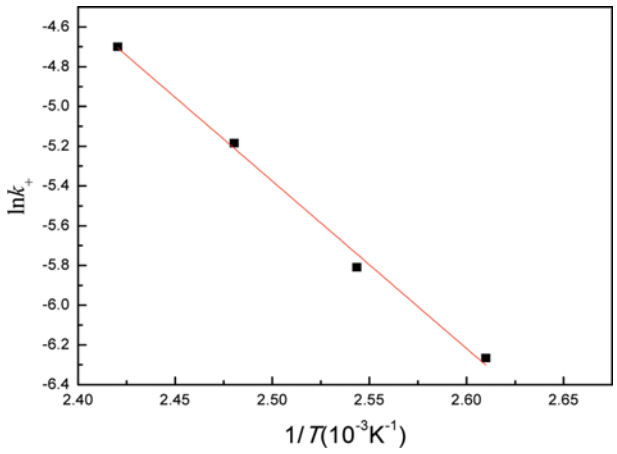

Fig. 13. Forward reaction rate constant k_+ versus temperature T.

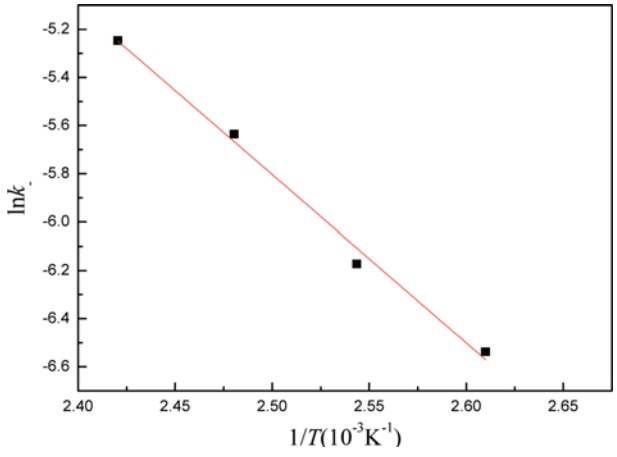

Fig. 14. Reverse reaction rate constant k_- versus temperature T.

$$k_+ = 6.4397\times10^6\exp\left(-\frac{70018.1}{RT}\right) \quad (16)$$

$$k_- = 1.1220\times10^5\exp\left(-\frac{57973.5}{RT}\right) \quad (17)$$

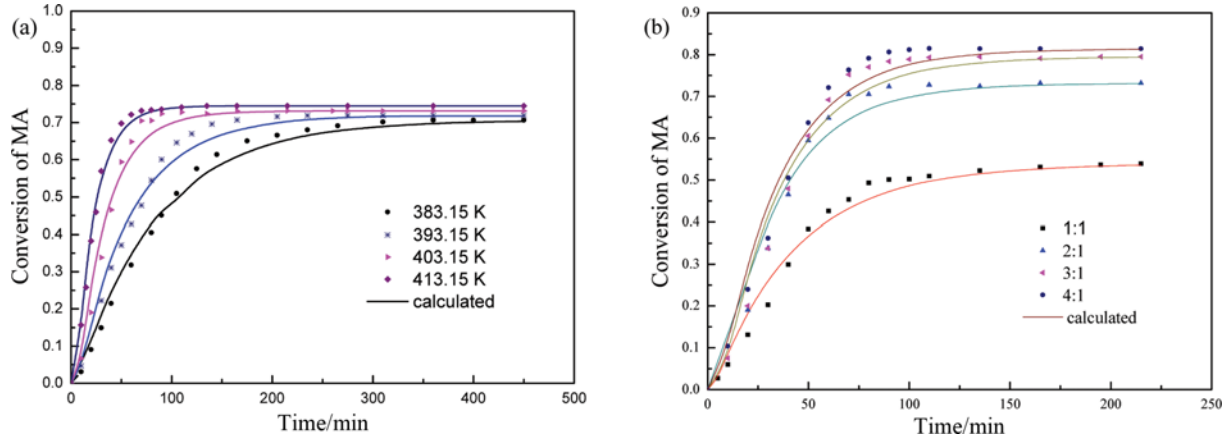

Fig. 15. Comparison between the calculated conversion of MA and the experimental data with (a) different temperature and (b) different feeding molar ratios.

E_a for the forward reaction is 70.018 kJ·mol^{-1}, which is higher than that obtained by TUNCER, 54.2 kJ·mol^{-1} [5]. The possible reason is that the catalytic activity of *p*-TSA is higher than SO_4^{2-}/TiO_2 in the present study. *p*-TSA catalyst shows high catalytic efficiency due to a large number of hydrogen ions. And the reaction rate over *p*-TSA catalyst was higher compared with reaction rate obtained over SO_4^{2-}/TiO_2.

Fig. 15 shows the comparison between calculated and experimental values of the conversion of MA with (a) different temperature and (b) different feeding molar ratios. According to the reaction mechanism, the model shows that the kinetic equation of esterification and kinetic parameters can describe the process of esterification reaction.

CONCLUSIONS

Sulfated titania (SO_4^{2-}/TiO_2) was prepared, and the results of characterization show that the prepared catalyst possesses super acidity and good stability. A kinetic study of esterification of myristic acid with isopropanol was performed in a batch reactor using SO_4^{2-}/TiO_2 as catalyst. The equilibrium conversion of myristic acid increased slightly with the increase of temperature. The experimental data were correlated with the pseudo-homogeneous second-order model. And the reaction rate constants, activation energy and frequency factor were determined. The calculated and experimental values were in good agreement.

ACKNOWLEDGEMENTS

We acknowledge the financial support for this work from the National Natural Science Foundation of China (Nos. 21576053, 91534106, and 21306025), the International S&T Cooperation Program of China (No. 2013DFR90540), the New Century Excellent Talents in Fujian Province University (JA12014), the Natural Science Fund for Distinguished Young Scholars of Fujian Province (2014J06004), Technology Development Fund of Fuzhou University (2012-XQ-7) and the Talent foundation of Fuzhou University (XRC-1448).

NOMENCLATURE

A : pre-exponential factor [L·min^{-1}·mol^{-1}]
AD : the acidity of the sample [mgKOH·g^{-1}]
AD_0 : the initial acidity of the sample [mgKOH·g^{-1}]
C : concentration [mol·L^{-1}]
C_{NaOH} : the concentration of NaOH [mol·L^{-1}]
E_a : activation energy [J·mol^{-1}]
ΔH : activation energy [J·mol^{-1}]
k_+ : forward reaction rate constant [L·mol^{-1}·min^{-1}]
k_- : reverse reaction rate constant [L·mol^{-1}·min^{-1}]
K_{eq} : equilibrium constant [dimensionless]
m : the weight of sample [g]
M_A : the molecular weight of myristic acid [g·mol^{-1}]
r : reaction rate [mol·L^{-1}·min^{-1}]
R_n : the molar ratio of isopropanol to myristic acid [dimensionless]
V_{NaOH} : the volume of NaOH [ml]
X_A : the conversion of MA [dimensionless]

Subscripts
1, 2, 3 : forward reaction of steps 1, 2 and 3 in Fig. 2
_1, _2, _3 : reverse reaction of steps 1, 2 and 3 in Fig. 2
A : myristic acid
B : isopropanol
R : isopropyl myristate

Superscripts
cal : calculated value
exp : experiment data

REFERENCES

1. Pattison and E. Scott, *Fatty Acids and Their Industrial Applications*, M. Dekker, Publications, New York (1968).
2. Y. Pouilloux, S. Abro, C. Vanhove and J. Barrault, *J. Mol. Catal. A: Chem.*, **149**, 243 (1999).
3. G. C. Gervajio and F. Shahidi, Bailey's Industrial Oil and Fat Products, book/10.1002/047167849X published online (www.interscience.wiley.com).
4. M. C. De Jong, R. Feijt, E. Zondervan, T. A. Nijhuis and A. B. de Haan, *Appl. Catal. A: Gen.*, **365**, 141 (2009).
5. T. Yalcinyuva, H. Deligoz, I. Boz and M. A. Gurkaynak, *Int. J. Chem. Kinet.*, **40**, 136 (2008).
6. L. D. Corinne and M. Zephirin, *Appl. Catal. A: Gen.*, **204**, 223 (2000).
7. M. Mazzotti, B. Neri, D. Gelosa, A. Kruglov and M. Morbidelli, *Ind. Eng. Chem. Res.*, **36**, 3 (1997).
8. R. Tesser, L. Casale, D. Verde, M. Di Serio and E. Santacesaria, *Chem. Eng. J.*, **157**, 539 (2010).
9. M. Berrios, J. Siles and M. Martìn, *Fuel*, **86**, 2383 (2007).
10. K. Srilatha, N. Lingaiah, D. B. L. A. Prabhavathi, R. B. N. Prasad, S. Venkateswar and S. S. Prasad, *Appl. Catal. A: Gen.*, **365**, 28 (2009).
11. Y. Sun, S. Ma, Y. Du, L. Yuan, S. Wang and J. Yang, *J. Phys. Chem. B.*, **109**, 2567 (2005).
12. V. V. Brei, *Theor. Exp. Chem.*, **41**, 165 (2005).
13. S. S. Hosseini and E. Sodagar, *C. R. Chim.*, **16**, 229 (2013).
14. J. L. Ropero-vega, A. Aldana-Pérez, R. Gómez and M. E. Nino-Gómez, *Appl. Catal. A: Gen.*, **379**, 24 (2001).
15. M. G. Kulkarni, R. Gopinath, L. C. Meher and A. K. Dalai, *Green Chem.*, **8**, 1056 (2006).
16. C. M. Garcia, S. Teixeira, L. L. Marciniuk and U. Schuchardt, *Bioresour. Technol.*, **99**, 6608 (2008).
17. B. Fu, L. Gao, L. Niu, R. Wei and G. Xiao, *Energy Fuel*, **23**, 569 (2009).
18. D. Rattanaphra, A. Harvey and P. Srinophakun, *Top. Catal.*, **53**, 773 (2010).